Stepwise Modulation of Neurokinin-3 and Neurokinin-2 Receptor Affinity and Selectivity in Quinoline Tachykinin Receptor Antagonists

Frank E. Blaney,*,† Luca F. Raveglia,*,‡ Marco Artico,‡ Stefano Cavagnera,‡ Catherine Dartois,§ Carlo Farina,‡ Mario Grugni,‡ Stefania Gagliardi,‡ Mark A. Luttmann,|| Marisa Martinelli,‡ Guy M. M. G. Nadler,§ Carlo Parini,‡ Paola Petrillo,⊥ Henry M. Sarau,|| Mark A. Scheideler,⊥ Douglas W. P. Hay,|| and Giuseppe A. M. Giardina*,‡

Department of Computational & Structural Sciences, SmithKline Beecham Pharmaceuticals, New Frontiers Science Park, Third Avenue, Harlow, Essex, England CM19 5AW, Departments of Medicinal Chemistry and Neurobiology Research, SmithKline Beecham S.p.A., Via Zambeletti, 20021 Baranzate, Milano, Italy, SmithKline Beecham Laboratoires Pharmaceutiques, Unité de Recherche, 4, rue du Chesnay−Beauregard, Boite Postale 96205, F-35762 St. Gregoire, France, and Department of Pulmonary Biology, SmithKline Beecham Pharmaceuticals, 709 Swedeland Road, King of Prussia, Pennsylvania 19406-0939

Received November 27, 2000

A stepwise chemical modification from human neurokinin-3 receptor (hNK-3R)-selective antagonists to potent and combined hNK-3R and hNK-2R antagonists using the same 2-phenylquinoline template is described. Docking studies with 3-D models of the hNK-3 and hNK-2 receptors were used to drive the chemical design and speed up the identification of potent and combined antagonsits at both receptors. (*S*)-(+)-*N*-(1-Cyclohexylethyl)-3-[(4-morpholin-4-yl)piperidin-1-yl]methyl-2-phenylquinoline-4-carboxamide (compound **25**, SB-400238: hNK-3R binding affinity, $K_i = 0.8$ nM; hNK-2R binding affinity, $K_i = 0.8$ nM) emerged as the best example in this approach. Further studies led to the identification of (*S*)-(+)-*N*-(1,2,2-trimethylpropyl)-3-[(4-piperidin-1-yl)piperidin-1-yl]methyl-2-phenylquinoline-4-carboxamide (compound **28**, SB-414240: hNK-3R binding affinity, $K_i = 193$ nM; hNK-2R binding affinity, $K_i = 1.0$ nM) as the first hNK-2R-selective antagonist belonging to the 2-phenylquinoline chemical class. Since some members of this chemical series showed a significant binding affinity for the human μ-opioid receptor (hMOR), docking studies were also conducted on a 3-D model of the hMOR, resulting in the identification of a viable chemical strategy to avoid any significant μ-opioid component. Compounds **25** and **28** are therefore suitable pharmacological tools in the tachykinin area to elucidate further the pathophysiological role of NK-3 and NK-2 receptors and the therapeutic potential of selective NK-2 (**28**) or combined NK-3 and NK-2 (**25**) receptor antagonists.

Introduction

The mammalian tachykinins—or neurokinins—including substance P (SP), neurokinin A (NKA), and neurokinin B (NKB), are a family of small peptides widely distributed in the central and peripheral nervous systems.[1] They produce an array of biological responses, including smooth muscle contraction and relaxation, vasodilation, activation of the immune system, regulation of pain transmission and neurogenic inflammation, and they have been proposed to play a pathophysiological role in a range of CNS and peripheral disorders, including migraine, depression, anxiety, emesis, asthma, and irritable bowel disease (IBD). These effects are mediated by specific 7 transmembrane G-protein coupled receptors (7 TM-GPCRs). The three tachykinins are able to activate all the receptors, although SP has the highest affinity for the neurokinin-1 receptor (NK-1R), NKA for the NK-2R, and NKB for the NK-3R. A broad background on the main biological aspects, profiles of neurokinin receptors and neurokinin receptor antagonists, and an extensive description of the lead generation and lead optimization processes in the discovery of the neurokinin receptor antagonists are given in recently published reviews.[1−7]

In recent years an outstanding number of publications have appeared in the literature describing both diverse chemical classes and specific compounds as selective antagonists of the NK-1, NK-2, and NK-3 receptors.[2,3,6] In contrast, there has been minimal information in the primary literature with regard to combined tachykinin receptor antagonists; however, in the patent literature, many nonselective tachykinin antagonists are claimed.[8] The rationale of synthesizing combined antagonists for the neurokinin receptors is mainly based on the potential synergistic effect associated with a multiple receptor interaction.[4,6] In particular, with regard to the NK-2 and NK-3 receptors, the potential for synergistic pharmacological effects is supported by the different locations of the two receptors. By its strategic location at the ganglia of parasympathetic nerves,[9,10] the NK-3R has the potential to influence the release, and thus the effect, of several rather than one neurotransmitter. Accordingly, an NK-3R antagonist would be expected to have therapeutic activity in pathological conditions

* To whom correspondence should be addressed. Phone: +39 02 3806-2265. Fax: +39 02 3806 2606. E-mail: giuseppe_giardina@sbphrd.com.
† Department of Computational & Structural Sciences, SmithKline Beecham Pharmaceuticals.
‡ Department of Medicinal Chemistry, SmithKline Beecham.
§ SmithKline Beecham Laboratoires Pharmaceutiques.
|| Department of Pulmonary Biology, SmithKline Beecham Pharmaceuticals.
⊥ Department of Neurobiology Research, SmithKline Beecham.

10.1021/jm000501v CCC: $20.00
Published on Web 04/25/2001

Chart 1. Chemical Structure of Compound 1

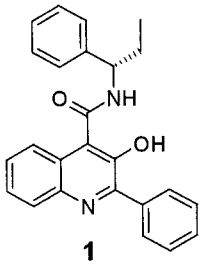

1

that have a significant neuronal component. NK-2R is found on end-organs, such as airway, bladder, and gastrointestinal (GI) tract smooth muscles.[9] Pulmonary, bladder, and GI tract disorders may therefore be the main potential therapeutic targets for combined NK-3 and NK-2 receptor antagonists.

In principle it should be possible to test the hypothesis of pharmacological synergism by utilizing a combination of two molecules, a selective NK-3R antagonist and a selective NK-2R antagonist. The issue associated with this approach lies primarily in the likely different pharmacokinetic profiles of the two compounds. An alternative, more attractive approach would be to test a single compound possessing combined NK-2R/NK-3R antagonist activity and to compare its effects with those of selective receptor antagonists.

The aim of this publication is to describe how the chemical structure of quinoline-based selective NK-3R antagonists, exemplified by (*S*)-(−)-*N*-(1-phenylpropyl)-3-hydroxy-2-phenylquinoline-4-carboxamide (**1**, SB-223412, talnetant, Chart 1),[11] was modified in a stepwise manner to obtain combined NK-3 and NK-2 receptor antagonists or selective NK-2R antagonists without major changes of the chemical template.

Chemical synthesis (Scheme 1), physicochemical properties (Table 1), and radioligand binding affinities (Table 2) of compounds **6**−**8**, **10**−**19**, **21**, and **23**−**28** will be detailed.

Moreover, novel 3D models of the human NK-3, NK-2, and μ-opioid receptors and docking hypotheses for the selective and combined ligands will be described. Inputs from these models were key drivers in the stepwise optimization process mentioned above.

Chemistry

The synthesis of compounds **6**−**28** was straightforward because they were all derived from a common key intermediate (3-bromomethylquinoline derivative **4**, Scheme 1), which could be easily produced in large amounts by radical bromination of methyl 3-methyl-2-phenylquinoline-4-carboxylate (**3**) with *N*-bromosuccinimide (NBS) in refluxing MeCN and in the presence of a catalytic amount of dibenzoylperoxide. Compound **3** in Scheme 1 could in turn be prepared by simple esterification of the corresponding, commercially available carboxylic acid (**2**, [CAS 43071-45-0]); this esterification was found to increase the yields of the bromination step with respect to the same reaction directly performed on the carboxylic acid. Nucleophilic displacement of the reactive benzyl bromide by a variety of secondary amines (R−H in Scheme 1) in THF in the presence of diisopropylethylamine (DIEA) at a temperature ranging from 20 to 50 °C afforded compounds of formulas **5a**−**j**. Acidic hydrolysis in refluxing 6 N HCl, and a subsequent coupling reaction with the appropriate primary amines (R_1−H) in THF/DCM in the presence of *O*-benzotriazol-1-yl-*N*,*N*,*N*′,*N*′-tetramethyluronium-hexafluorophosphate (HBTU) as a condensing agent and TEA gave the desired amides **6**−**9**, **11**−**20**, **22**, and **24**−**28** of general formula I in Table 1.

Compounds **10**, **21**, and **23** were obtained by fmoc deprotection of the corresponding compounds **9**, **20**, and **22**, respectively, in MeCN at room temperature in the presence of piperidine.

Pharmacology

Radioligand Binding Assays. Neurokinin receptors binding assays were performed with crude membranes from Chinese hamster ovary (CHO) cells expressing the hNK-3, hNK-2, or hNK-1 receptors (hNK-3-CHO, hNK-2-CHO, and hNK-1-CHO, respectively) as detailed previously.[12−14] For NK-3R competition binding studies, [^{125}I]-[MePhe^7]-NKB binding to hNK-3-CHO membranes was performed using the procedure of Sadowski and co-workers[15] as described previously.[14] For NK-2R competition binding studies, [^{125}I]-NKA binding to hNK-2-CHO membranes was performed essentially as described by Aharony et al.[16] Competition binding studies for the NK-1R were performed on hNK-1-CHO membranes essentially as described by Payan et al.[17]

Stable expressions of human δ- (hDOR) and human μ-opioid receptors (hMOR) in CHO cell lines and of κ-opioid receptors (hKOR) in human embrionic kidney (HEK-293) cell lines have been performed in house, using pCDN vectors.[18] Receptor binding assays were performed in membranes prepared by lysis in hypotonic phosphate buffer[19] using the method described by Kotzer et al.[18] with minor modifications. Briefly, the following radioligands were utilized: [^{3}H]-[D-Ala^2,MePhe^4,Gly-ol^5]enkephalin ([^{3}H]-DAMGO, New England Nuclear, Belgium), [^{3}H]-[D-Ala^2,D-Leu^5] enkephalin ([^{3}H]-DADLE, New England Nuclear, Belgium), and [^{3}H]-U-69593 (Amersham, Italia) to label μ-, δ-, and κ-opioid receptors, respectively.

Concentration−response curves in the hNK-3-CHO, hNK-2-CHO, and hMOR-CHO binding assays were run using duplicate samples for compounds **1**, **6**−**8**, **10**−**19**, **21**, and **23**−**28**; among them, compounds that gave an IC_{50} binding affinity lower than 2.5 μM in the first experiment were run in three to five independent experiments ($n = 3-5$).

The percent inhibition of specific binding in the NK-3 and NK-2 receptor binding assays was determined for each concentration of the compounds and the IC_{50}, defined as the concentration required to inhibit 50% of the specific binding, obtained from concentration−response curves. Values reported in Table 2 are the apparent inhibition constant (K_i), which was calculated from the IC_{50} as described by Cheng and Prusoff.[20]

Compounds **1**, **6**, and **24** were studied in the hNK-1-CHO binding assay, while compounds **1**, **25**, and **28** were evaluated in the hKOR and hDOR binding assays.

Results and Discussion

1. Modeling the Neurokinin NK-2/NK-3 and the μ-Opioid Receptors. For some years now, we[21] and others[22] have described models of G protein-coupled

Scheme 1. Synthesis of Compounds **6**−**28**[a]

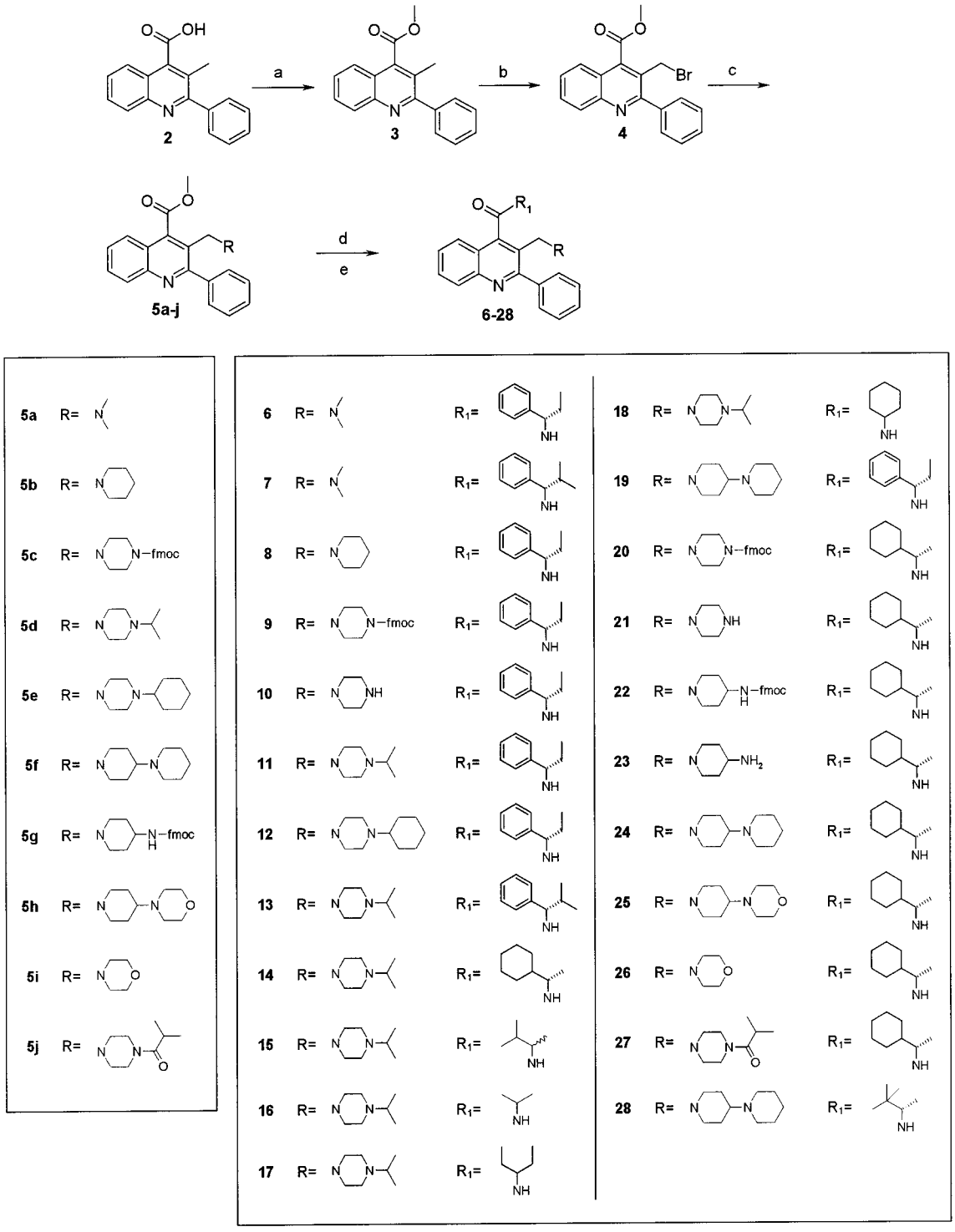

[a] Reagents: (a) $(COCl)_2$, DCM, room temperature, 1 h; MeOH, DCM, room temperature, 18 h; (b) NBS, dibenzoylperoxide, CH_3CN, reflux, 28 h; (c) RH (a secondary amine), DIEA, THF, room temperature to 50 °C, overnight; (d) HCl (6 N), reflux, 4 h; HBTU, R_1H (a primary amine), TEA, THF/DCM, 25 °C to reflux, 18 h; (e) (only for compounds **9**, **20**, and **22**) piperidine, CH_3CN, room temperature, overnight.

receptors (GPCRs), which were initially based on the transmembrane helix packing bundle of bacteriorhodopsin (BR). These were modified when the early 9 Å cryoelectron diffraction map of bovine rhodopsin[23] suggested that the relative tilt of the helices differed from that of BR. A major breakthrough was reported in 1997 by Unger et al,[24a] when a 6 Å electron density map of rhodopsin was described as a series of slices at 4 Å intervals through the membrane. The implications of this, particularly the unexpected tilt angle of transmembrane helix 3 (TM3), led us to conclude that a totally new template structure was necessary before further ligand design work could reliably be performed.

It was assumed in the description below that the same helix packing arrangement is present in all GPCR

Table 1. Physical Properties of Compounds **6**−**8**, **10**−**19**, **21**, and **23**−**28** of General Formula **I**

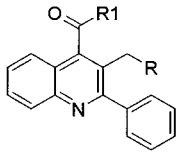

I

Compd	R	R_1	formula	mp, °C	anal.	$[\alpha]_D^{20}$ (c=0.5, MeOH)
6	NMe_2	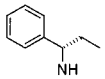	$C_{28}H_{29}N_3O$ 2 HCl	168-170	C,H,N,Cl	-25.3[a]
7	NMe_2	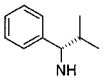	$C_{29}H_{31}N_3O$	117-120	C,H,N	-63.0
8		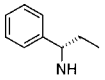	$C_{31}H_{33}N_3O$ 2 HCl	140 dec.	C,H,N,Cl	22.5
10		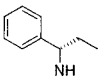	$C_{30}H_{32}N_4O$	95-98	C,H,N	-47.3[a]
11		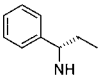	$C_{33}H_{38}N_4O$ 3 HCl	120 dec.	C,H,N,Cl[c]	-38.0
12	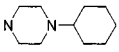	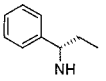	$C_{36}H_{42}N_4O$ 3 HCl	262-264	C,H,N,Cl	-49.0
13		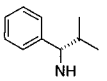	$C_{34}H_{40}N_4O$	125-130	C,H,N	-69.2
14			$C_{32}H_{42}N_4O$ 3 HCl	180-183	C,H,N,Cl[d]	19.5
15			$C_{29}H_{38}N_4O$ 3 HCl	204-206	C,H,N,Cl	--
16			$C_{27}H_{34}N_4O$ 3 HCl	198-200	C,H,N,Cl	--
17			$C_{29}H_{38}N_4O$ 3 HCl	235-238	C,H,N,Cl	--
18			$C_{30}H_{38}N_4O$	161-163	C,H,N	--
19	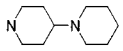	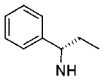	$C_{36}H_{42}N_4O$ 3 HCl	182-185	C,H,N,Cl[e]	-4.1
21			$C_{29}H_{36}N_4O$	112-114	C,H,N	20.5[a]
23	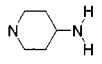	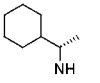	$C_{30}H_{38}N_4O$	140-145	C,H,N	nd
24	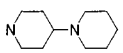	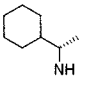	$C_{35}H_{46}N_4O$ 3 HCl	180-184	C,H,N,Cl	6.9
25	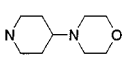	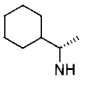	$C_{34}H_{44}N_4O_2$	136-138	C,H,N	11.9[b]
26		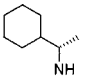	$C_{29}H_{35}N_3O_2$	180-181	C,H,N	14.3[b]

Table 1 (Continued)

Compd	R	R_1	formula	mp, °C	anal.	$[\alpha]_D^{20}$ (c=0.5, MeOH)
27	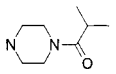		$C_{33}H_{42}N_4O_2$	151-153	C,H,N[f]	10.4[b]
28	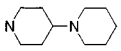		$C_{33}H_{44}N_4O$	185-187	C,H,N	26.8[b]

[a] $c = 1$, MeOH. [b] $c = 0.25$, MeOH; nd = not determined. [c] Cl: calcd, 17.26; found, 16.78. [d] C: calcd, 63.21; found, 63.88. H: calcd, 7.46; found, 7.03. Cl: calcd, 17.49; found,17.01. [e] C: calcd, 65.90; found, 65.44. [f] C: calcd, 75.25; found, 75.67.

Table 2. Binding Affinities of Compounds **1**, **6**−**8**, **10**−**19**, **21**, and **23**−**28** at Cloned hNK-3, hNK-2, and hMOR Receptors

compd	binding affinities (K_i, mean ± SEM (nM)) hNK-3	hNK-2	hMOR	hNK-2/hNK-3 receptor selectivity ratio
1[a,b]	1.4 ± 0.2	144 ± 22	1860 ± 560	103
6[a]	2.2 ± 0.3	172 ± 18	1680 ± 480	78
7	3.3 ± 1.1	51.6 ± 18.8	>2500	16
8	7.0 ± 1.1	276 ± 99	>2500	39
10	4.7 ± 1.0	22.2 ± 3.6	203 ± 12	4.7
11	1.8 ± 0.4	5.7 ± 0.5	98.6 ± 10.3	3.1
12	1.2 ± 0.1	1.6 ± 0.1	15.8 ± 0.6	1.3
13	1.2 ± 0.1	1.5 ± 0.2	120 ± 13	1.2
14	1.9 ± 0.4	0.7 ± 0.1	195 ± 59	0.4
15	454 ± 129	9.2 ± 0.8	*d*	0.02
16	>12000	811 ± 211	*d*	<0.1
17	1210 ± 180	18.5 ± 9.3	*d*	0.015
18	1250 ± 30	4.2 ± 0.3	226 ± 15	0.003
19	1.5 ± 0.4	4.6 ± 0.4	919 ± 89	3.1
21	3.4 ± 0.6	2.4 ± 0.4	172 ± 6.8	0.7
23	31.2 ± 2.4	33.0 ± 8.9	1780 ± 450	1.1
24[a,c]	1.7 ± 0.1	0.6 ± 0.1	1320 ± 170	0.3
25[b]	0.8 ± 0.1	0.8 ± 0.1	>2500	1
26	4.6 ± 0.8	6.1 ± 0.5	>2500	1.3
27	1.4 ± 0.3	1.2 ± 0.1	>2500	0.9
28[b]	193 ± 48	1.0 ± 0.2	≥2000	0.005

[a] Compounds **1**, **6**, and **24** were assessed for their ability to displace [^{3}H]-SP binding from hNK-1-CHO membranes with the method described in ref 17; they were devoid of any significant effects up to concentration of 100 μM. [b] Compounds **1**, **25**, and **28** were assessed for their ability to displace [^{3}H]-U69593 binding from HEK membranes transfected with the hKOR and [^{3}H]-DADLE from CHO membranes transfected with the hDOR and were devoid of any significant effects up to concentration of 2.5 μM. [c] A representative member of this chemical series, compound **24**, was assessed for its cellular functional antagonist activity in the NKB-induced CA^{2+} mobilization assay in HEK cells stably expressing the hNK-3R (K_B = 2.6 nM, pA_2 = 8.7) following the method described in ref 12, and in the NKA-induced Ca^{2+} mobilization assay in HEK cells stably expressing the hNK-2R (K_B = 9.9 nM, pA_2 = 8.0); these data confirm the well-known antagonist properties of quinoline-based NK-3 and NK-2 receptor ligands.[11,14] [d] Not determined.

family 1 receptors. Therefore, ligand binding and site-directed mutagenesis data were collated from a number of different receptors. As a starting point for the construction of the new template, a computer program was written that would convert the electron density slice images into accurate three-dimensional representations (see Experimental Section for details of the algorithm used). These density contours were then used to define the axes of the helices in a manner similar to that described by Baldwin.[24b] The helix sequences derived from hydropathy plots[25] were then manually folded around these axes, assuming the standard values of −59° and −44° for ϕ and ψ in a hydrophobic helix,[26] but adjusting these where necessary to take account of irregularities in the helical axes.

Use was made at this stage of the program Helanal[27] developed by us some years ago to define the interior face and the hydrophobic exposure of a transmembrane helix. This defines the conservation moment arising from a multiple sequence alignment of closely related proteins, as a Fourier power spectrum, using the algorithm originally described by Donnelly et al.[28] The moment is then mapped onto a color-coded helical wheel. A set of rules are used to define a hydrophobic arc on the wheel, which gives an indication of the degree to which the helix is exposed to the lipid bilayer. When this is used together with site-directed mutagenesis information from a variety of sources, the helical domains were folded around the axes described above. Density around TM6 suggests a strongly bent helical structure that corresponds to a kink produced by the highly conserved proline. This places two highly conserved aromatic residues (phenylalanine **F**261 and tryptophan **W**265 of bovine rhodopsin) on the inside of the helix bundle. In the aminergic receptors, the conserved TM6 proline is followed by two phenylalanine residues. The orientation in the model suggests that the latter of these is inward-facing, whereas the former is interhelical. Mutation studies of these phenylalanines in the 5HT2a receptor[29] have shown that it is the latter residue that is mainly involved in ligand binding, in keeping with the model.

TM3 was placed with the cysteine at the extracellular side oriented toward TM5, in anticipation of the formation of a disulfide bond with the second extracellular loop between TM4 and TM5. The seventh residue below this cysteine has been identified from mutagenesis work[30] as the key TM3 binding residue for many receptors; e.g., it is an aspartate in the aminergic, opioid, and several peptide receptors and binds to a protonated amino group in the natural ligands. As a result of the cysteine placement, this was also oriented toward the TM5−TM6 region, which has again been identified from mutagenesis studies[29,31] to be crucial for the binding of small molecule agonists such as the monoamines. This orientation of TM3 is quite different from the model described by Baldwin,[24b] where the above residues in TM3 are oriented more toward TM2 and TM7.

TM4 contains a highly conserved tryptophan found in both family 1 and family 2 receptors, which was predicted to be inward-facing by Helanal. The unusual tilt of TM3 suggested that this trypyophan played a structural role, acting as a "wedge" packing against TM3

and forcing it through the middle of the bundle. TM4 was thus aligned with its axis in such a way that the tryptophan was stacked against a tryptophan (**W**126) of bovine rhodopsin in the intracellular half of TM3. The structural rather than binding role of the TM4 tryptophan has been confirmed in the muscarinic receptor where mutation to phenylalanine had no effect on ligand binding.[32]

As with TM6, a similar though less pronounced kink was observed in the helix axis of TM5. This was again aligned with the conserved proline in this region. Mutation studies in the adrenergic and dopamine receptors have suggested that two serine residues in TM5 are involved in agonist binding.[31] The helix was rotated to ensure that these residues were oriented toward the interior of the bundle. The density slice information has suggested that TM5 has relatively little interhelical interaction with TM4 and TM6 at the extracellular side. This is supported by SCAM mutations carried out on the dopamine D2 receptor,[33b] which show that all residues at the extracellular side of TM5 are relatively accessible. The main implication of this is that the assumed binding pocket between TM3, TM5, and TM6 is larger than in previous models.

The remaining three helices proved to be much harder to align with their axes. The main guidance here was that there is ample evidence suggesting that three highly conserved residues, an asparagine in TM1, an aspartate in TM2, and an asparagine in TM7, together form a hydrogen-bonded network that is involved in the functional response of family 1 GPCRs.[34] The placement of TM2 was carried out on the basis of an unusual double bend in the helix axis, which was attributed to the double glycine (**G**89/**G**90) in TM2 of rhodopsin. The conserved aspartate (**D**83) was oriented toward TM7. This then allowed placement of the TM7 asparagine (**N**302) within hydrogen-bonding distance of the aspartate. Much adjustment of the $\phi-\psi$ angles of TM7 was necessary to allow the lysine (**K**296) of rhodopsin to orient itself in a suitable rotamer into the bundle so that it could form the Schiff base with retinal. Finally, TM1 was placed by aligning the kink in the axis with proline (**P**53) in rhodopsin and rotating the helix so that the TM1 asparagine (**N**55) was oriented toward asparagine (**N**302) in TM7.

Models of the TM domains of numerous GPCRs have been built on the basis of this template, using the automated program GPCR_Builder.[35] The resulting structures were all subjected to several rounds of side chain conformational refinement using the Karplus rotamer library[36] option in Quanta,[37] prior to their final minimization with CHARMm.[38] Comparison of the models with experimental data is generally very good. For example the dopamine D2 model is in agreement with the SCAM data published by Javitch[33] and the 5HT2 models explain most of the published mutagenesis experiments.[29,39] What was particularly encouraging was that the model of the double histidine mutant of the NK-1R, constructed by Elling et al.[40] in their work on GPCR zinc binding sites, exhibited a near-perfect zinc−histidine triad arrangement between TM5 and TM6.

The NK-2, NK-3, and μ-opioid receptor models were built from the template as described above and used in initial docking studies of the quinoline antagonists. It quickly became clear that these ligands would have to extend into the extracellular domains. The extracellular loops were therefore added using a new semiautomated procedure (see Experimental Section for details of this method). Initially the long second loop between TM4 and TM5 was built with its disulfide bond between the cysteine at the top of TM3 and the cysteine in the loop. The shorter TM2−TM3 and TM6−TM7 loops were then added afterward.

2. Structure−Activity Relationships (SARs, Table 2). Structure−activity considerations on a large set of selective NK-3R antagonists reported in a previous paper in this journal[11] identified position 3 of the quinoline nucleus as the best point for chemical variation. This observation prompted a broad investigation of substitution at this position with the aim of improving the affinity for the NK-2R. In addition, a particular focus was given to tertiary amines with the objective of improving water solubility and brain penetration (compared to the same parameters obtained for compound **1**).[12]

A conformational analysis study on the rotatable bonds of 2,3,4-trisubstituted quinolines revealed, not suprisingly, that these compounds are very rigid. The ortho substitution in the quinoline means that the 2-phenyl substituent of the series sits well out of plane with the bicyclic ring. For the same reason, the 4-amido group adopts one of two narrow ranges of conformations that are essentially orthogonal to the quinoline ring and 180° apart from each other. This rigidity limited the number of rotational conformers that needed to be examined during docking studies in the receptor models.

Compound **1** was manually placed in the NK-3R model in the cavity between TM3, TM4, TM5, TM6, and TM7. A variety of different starting orientations were used. Care was taken with this and other ligands to ensure that only low-energy rotational conformers were considered during the initial placements. Each starting orientation was then minimized fully using the CHARMm program. Where likely hydrogen bonding or charged interactions were identified, during the initial placements, no distance constraints were applied to the first stages of the minimization procedure. It became clear that one particular binding orientation explained much of the previously observed SAR of these compounds.[11,14] In Figure 1, it can be seen that the essential quinoline nitrogen forms a hydrogen bond with a tyrosine in TM6 (**Y**315). The quinoline ring itself is surrounded by a number of other aromatic residues, including a tyrosine (**Y**256) in TM5 and a phenylalanine (**F**319) and histidine (**H**316) in TM6. This histidine can also form a hydrogen bond with the amide hydrogen on the 4-substituent of the quinoline. The 2-phenyl substituent is forced to sit orthogonal to the quinoline ring, in keeping with the conformational analysis results, and fits into a very tight pocket bounded by an asparagine (**N**162) and proline (**P**165) in TM3, a phenylalanine (**F**234) in the second extracellular loop, and a tyrosine (**Y**338) and phenylalanine (**F**342) in TM7. The tight dimensions of this pocket explain previous observations that only very limited substitution (a 2-fluoro group) is tolerated on this ring.[14]

With the exception of phenylalanine (**F**234), all these residues are conserved in the NK-2R. However, docking

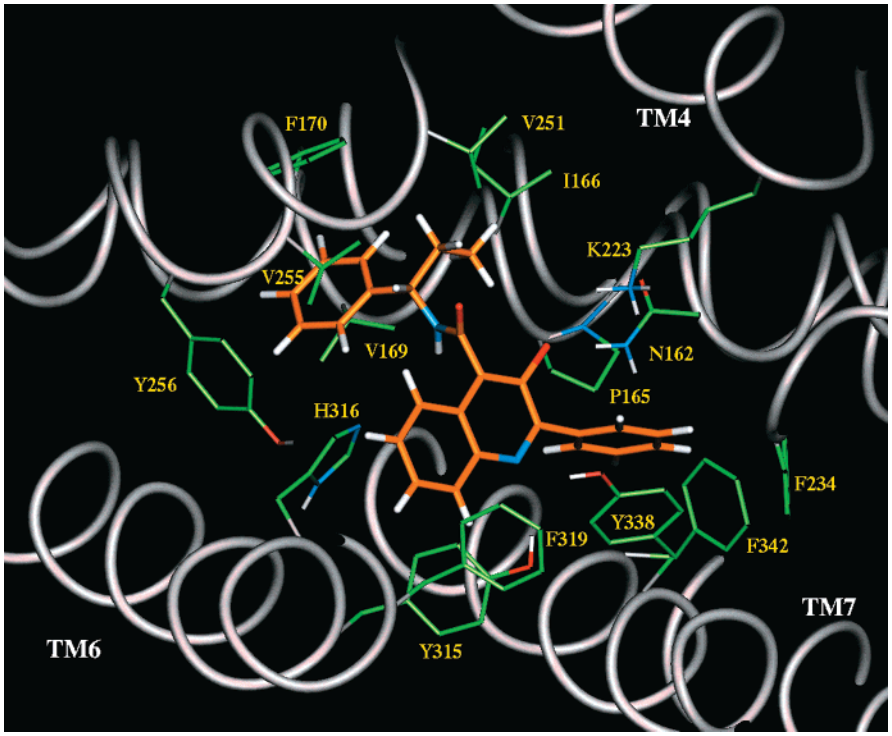

Figure 1. Compound **1** bound in the NK-3 receptor model. Most residues have been removed for clarity.

		TM1	IC1	TM2
NK3R_HUMAN	TNQFVQPSWRIA	LWSLAYGVVVAVAVLGNLIVIWIIL	AHKRMRTV	TNYFLVNLAFSDASMAAFNTLVNFIYALHSEW
NK2R_HUMAN	ITAFSMPSWQLA	LWAPAYLALVLVAVTGNAIVIWIIL	AHRRMRTV	TNYFIVNLALADLCMAAFNAAFNFVYASHNIW
	* ***:**	**: ** .:* *** ** *******	**:*****	****:****:* .*****: .**:** *. *

	EC1	■ ▼ ▼▼ ▼▼ TM3	IC2	TM4 ▼ ▼▼
NK3R_HUMAN	YFGANY	CRFQNFFPITAVFASIYSMTAIAVDRYMAI	IDPLKPRLSATAT	KIVIGSIWILAFLLAFPQCLYSKT
NK2R_HUMAN	YFGRAF	CYFQNLFPITAMFVSIYSMTAIAADRYMAI	VHPFQPRLSAPST	KAVIAGIWLVALALASPQCFYSTV
	*** :	* ***:*****:*.********.******	:.*::*****.:*	* **..**::*: ** ***:**..

	▼■▼ EC2	▼ ▼ ▼▼ ▼ TM5	EC3
NK3R_HUMAN	KVMPGRTLCFVQWPE--GPKQHFTY	HIIVIILVYCFPLLIMGITYTIVG	ITLWGGEIPGDTCD-KYHEQLKAKRK
NK2R_HUMAN	TMDQGATKCVVAWPEDSGGKTLLLY	HLVVIALIYFLPLAVMFVAYSVIG	LTLWRRAVPGHQAHGANLRHLQAKKK
	.: * * *.* *** * * : *	*::** *:* :** :* ::*:::*	:*** :**. .. .:*:**:*

	TM6 ▼▼ ▼	EC3	▼ ▼ TM7
NK3R_HUMAN	VVKMMIIVVMTFAICWLPYHIYFILTAI	YQQLNRWK	YIQQVYLASFWLAMSSTMYNPIIYCCLN
NK2R_HUMAN	FVKTMVLVVLTFAICWLPYHLYFILGSF	QEDIYCHK	FIQQVYLALFWLAMSSTMYNPIIYCCLN
	.** *::**:**********:**** ::	::: *	:******* ********************

Figure 2. Sequence alignment of the NK-3 and NK-2 receptors showing the various regions used in the modeling (TM = transmembrane helix; EC = extracellular loop; IC = intracellular loop). The residues involved in binding are in bold below the ▼ symbol. Conserved residues are indicated by the ∗ symbol below the alignment. The cysteines of the disulfide bond are below the ■ symbol.

of **1** into the NK-2R model revealed some interesting differences between the two receptors; these differences are highlighted by the alignment of the two sequences shown in Figure 2. In both models, the 3-hydroxy substituent forms a hydrogen bond with the TM3 asparagine (**N**162). In the NK-3R, however, there is an additional strong electrostatic interaction with a lysine (**K**223) at the top (extracellular side) of TM4. Indeed it is likely that the acidic nature of the phenolic group would imply that it is ionized in the NK-3R, which would increase the strength of the interaction. The corresponding residue in the NK-2R, threonine (**T**171), is too small to make any interactions with the ligand. This would suggest that increasing the size of the 3-substituent, together with the introduction of suitable functionality in this substituent, should increase the affinity for the NK-2R. Thus, the selectivity of compound **1** for the NK-3R can be explained by the presence of this salt bridge alone.

Further differences between the two models can be seen in the binding pocket for the (*S*)-1-phenylpropyl amide substituent. In the NK-3R, this binds in a hydrophobic pocket bounded by isoleucine (**I**166), valine (**V**169), and phenylalanine (**F**170) in TM3 and by the valines (**V**251 and **V**255) and proline (**P**259) in TM5. In the NK-2R, valine (**V**169) is replaced by a methionine

and valine (**V**255) is replaced by an isoleucine. Again, this would suggest that subtle changes in the bulk of the amide substituent could affect the selectivity for the two receptors.

The proposed introduction of tertiary amino substituents at the 3-position was chemically facilitated by the possibility of utilizing a common key intermediate (the 3-bromomethylquinoline derivative **4**) that could be easily produced in large amounts and coupled with a set of diverse secondary amines in high yields.

Whereas the smallest tertiary amine (the dimethylamine) produced the moderately NK-3R selective compound **6** (hNK-2R/hNK-3R binding affinity ratio = 78), introduction of the piperidino group (compound **8**) decreased the selectivity by a factor of 2, thus resulting in a hNK-2R/hNK-3R receptor binding affinity ratio of 39. Docking of these compounds into the NK-2R model suggested that the protonated nitrogen of the 3-substituent could now form a hydrogen bond with the amide carbonyl in the side chain of asparagine (**N**110) in TM3. In the NK-3R, the same interaction can be seen, but in addition, it is likely that proton exchange occurs with the primary amino group of the TM4 lysine (**K**223). As predicted earlier, the increased bulk of the piperidine ring allows it to make favorable interactions with cysteine (hNK-2R **C**167) in TM4 and valine (hNK-2 **V**201) in TM5, thus increasing the affinity for the NK-2R.

One significant difference between the NK-2 and NK-3 receptor sequences (Figure 2) was the presence of a lysine (**K**180) located in the former receptor in the second extracellular loop, adjacent to the disulfide bond. In the NK-3R sequence, this amino acid is leucine. In our model of the NK-2R, this side chain could extend into the cavity toward the 3-substituent. In addition, the different lengths of the second extracellular loop in the two receptors resulted in a different orientation of the conserved histidine (hNK-2R **H**198) at the C-terminal end of this loop. In the NK-2R, this histidine is also pointing into the binding cavity. These observations suggested that a second polar substituent in the piperidine ring could improve the NK-2R affinity. Significantly, a considerable increase in the combined NK-2R/NK-3R receptor binding profile was obtained by introducing an extra basic nitrogen in the piperidine ring, producing the piperazine derivative **10**. Docking of this compound into the NK-2R model showed that the loop lysine (**K**180) would now form an interaction with the piperazine nitrogen. This compound showed a marked combined profile (hNK-3R binding affinity, K_i = 4.7 nM; hNK-2 binding affinity, K_i = 22.2 nM) with a hNK-2R/hNK-3R receptor binding affinity ratio of 4.7. The introduction of the second amino group meant that two possible protonated states would need to be considered in the modeling. Estimations of the relative basicities were made on the basis of the relative heats of formation of the isomers, as calculated by ab initio Hartree−Fock methods.[41] A second approach to this was to calculate the maximum positive electrostatic potential of the protonated isomer at the surface of this proton.[41] This follows from the fact that the more basic the nitrogen, the more polarized the NH bond of the cation will be, and hence, it will develop a more positive charge at the NH center. With compound **10**, the tertiary benzylic position was predicted to be more favored for protonation over the secondary piperazine nitrogen. N-alkylation of the piperazine might be expected to shift this equilibrium in favor of the nonbenzylic position. However, calculations showed that the tertiary piperazines still favored protonation at the benzylic position (albeit with a smaller energy difference), thus maintaining the interaction with the TM3 asparagine. While N-alkylation of the piperazine would not change the protonation site, examination of the models suggested that extension of an alkyl substituent into the cavity would pick up further hydrophobic interactions with the TM4 threonine (**T**171) and the loop histidine (**H**198) in the NK-2 receptor. N-alkylation at the piperazine ring with the i-Pr group (compound **11**) produced an approximate 3-fold increase in both hNK-3R (K_i = 1.8 nM) and hNK-2R (K_i = 5.7 nM) binding affinities over the unsubstituted piperazine **10**, resulting in a slightly increased combined profile (hNK-2R/hNK-3R binding affinity ratio of 3.1). As predicted, an even more pronounced effect was observed with compound **12** featuring the more bulky cyclohexyl group (hNK-2R/hNK-3R binding affinity ratio of 1.3).

Because compound **11** (and **12**) showed potent binding affinities at both receptors, further attention was focused on the role of the amidic portion while maintaining the i-Pr-piperazine group in position 3 of the quinoline nucleus. As has already been mentioned, there are subtle differences between the receptor models in this binding pocket. Accordingly, compounds **13**−**18** in Table 2 feature several amide variations. The first modification consisted of the simple replacement of the Et at the benzylic position with an i-Pr group, giving compound **13**, which showed a 3-fold increase in hNK-2R binding affinity. Thus, this compound had equivalent affinity at both receptors (K_i about 1 nM). Docking of this compound into the two receptor models showed that the increase in NK-2R affinity could readily be explained by the increased hydrophobic interaction of the bulkier isopropyl group with the unique TM3 methionine (**M**117). In the NK-3R model, the phenyl group of the 4-amido substituent is sandwiched between the two valines (**V**169 and **V**255) that are specific to this sequence. Replacement of these in the NK-2R by the larger methionine and isoleucine residues, respectively, suggested that increase in the hydrophobic bulk of the phenyl substituent would give an increased affinity for the NK-2R. Indeed a further increase in the hNK-2R binding affinity was obtained by replacing the phenyl ring with the cyclohexyl and, concomitantly, the Et with the Me group to give compound **14** (hNK-3R binding affinity, K_i = 1.9 nM; hNK-2R binding affinity, K_i = 0.7 nM). The larger hydrophobic cavity in the NK-3R would also suggest that reduction in size of the amide substituent would have a greater detrimental effect on binding than in the NK-2R. Replacement of the cyclohexyl group with i-Pr (**15**) produced a compound that, although less potent at both receptors, was clearly much more hNK-2R selective (hNK-2R/hNK-3R receptor binding affinity ratio of 0.02). Therefore, in agreement with the prediction from the docking studies, the data obtained for compounds **14** and **15** suggest that a decrease in the steric hindrance of substituents at the amidic nitrogen should be associated with a strong

decrease in the hNK-3R binding affinity while potentially maintaining an adequate hNK-2R component. To further test this hypothesis, we decided to introduce small alkyl symmetric groups, which led to the achiral compounds **16**−**18**. While replacement of the i-Pr group in compound **15** with the simple Me afforded a poorly active compound at both receptors (**16**), incorporation of the isopentyl group on the amidic nitrogen was clearly beneficial and provided compound **17** with a selectivity ratio of 0.015. The most hNK-2R selective compound was obtained by introducing a cyclohexyl group directly attached to the amidic nitrogen (**18**). This had an outstanding hNK-2R/hNK-3R receptor binding affinity ratio of 0.003 with a hNK-3R binding affinity of 1245 nM and hNK-2R binding affinity of 4.2 nM. Docking studies showed that the cyclohexyl group could interact with the TM3 methionine in the NK-2R but could not interact with the corresponding smaller valine in the NK-3R.

It is worth noting that this achievement of such good hNK-2R selectivity was made with a compound devoid of stereogenic centers, whereas previous literature evidence suggested that the presence of the stereogenic center in the amidic portion of the molecule was necessary for strong hNK-3R binding affinity in quinoline-based hNK-3R selective antagonists.[13,14]

In view of the potential in vivo use of some of the compounds described above, it was decided to profile them in a battery of receptor, ion channel, and enzyme assays, paying particular attention to the opioid receptor family. The reason for a specific opioid profile came from the observation that another NK-3R antagonist, (*R*)-(+)-*N*-{{3-[1-benzoyl-3-(3,4-dichlorophenyl)piperidin-3-yl]prop-1-yl}-4-phenylpiperidin-4-yl}-*N*-methylacetamide (SR 142,801, osanetant), albeit chemically unrelated, has been described as interacting with opioid receptors with IC_{50}s in the 0.1−1 uM range (human μ-opioid receptor binding affinity, $K_i = 480$ nM, in-house data).[42] As a result, compounds **10**−**14** and **18** showed human μ-opioid receptor binding affinities in the range 16−226 nM, whereas compounds **1** and **6**−**8** were devoid of any significant human μ-opioid receptor binding affinity.

From these results, it could be speculated that the μ-opioid receptor binding component was related to the presence of the second piperazine nitrogen (compare compound **10**, human μ-opioid binding affinity, $K_i = 203$ nM with compound **8**, human μ-opioid binding affinity, $K_i > 2.5$ μM). To study this further, compound **12**, which showed the greatest affinity for the human μ-opioid receptor (human μ-opioid $K_i = 15.8$ nM), was examined in detail in all three receptor models. Ab initio quantum calculations, carried out as described earlier, demonstrated that the preferred site of protonation was at the nonbenzylic nitrogen, although the difference between the two sites was calculated to be only 4.3 kcal (in the gas phase). An estimation of the difference in pK_a between the two protonated states using electrostatic potential calculations showed that they were quite close (ca. 0.4 kcal), which would suggest that they are in equilibrium. Docking studies with compound **12** in both the NK-2 and NK-3 receptors showed that with benzylic protonation, the protonated site formed a strong hydrogen bond to the TM3 asparagine, as previously described. On the other hand, only weak, nonspecific polar interactions were observed with the other protonated isomer. As with other opioid receptors, the overriding driving force for binding to human μ opioid is the interaction of the protonated nitrogen with a conserved aspartate on TM3 (human μ **D**149). The μ receptor does not have the TM3 asparagine or the TM6 tyrosine, which are essential residues for NK receptor binding, and it has a bulky tyrosine instead of the TM3 isoleucine in the phenylpropyl pocket. Thus, the μ receptor is believed to bind the compounds in a totally different manner. Docking studies of **12** in the human μ-opioid receptor model (Figure 3) showed that the protonated nitrogen at the nonbenzylic position could interact with the aspartate on TM3. The NH of the 4-amido substituent could still hydrogen-bond to the histidine at the top of TM6 (human μ **H**299), which is conserved in the three receptors. The molecule is essentially binding "upside down" compared to the NK receptor binding mode, with no major contributions other than a shape complementarity (see Figure 4). The opioid binding mode showed that the position and directionality of the protonated nitrogen were crucial. Further docking studies suggested that if the nitrogen of **12** was shifted into the cyclohexyl ring to give the 4-(piperidin-1-yl)piperidin-1-yl derivative **19**, then interaction with the TM3 aspartate in the μ-opioid receptor would be abolished without affecting its NK receptor binding.

To test this hypothesis compound **19** was synthesized. In perfect agreement with the docking study prediction, **19** displayed a human μ-opioid receptor binding affinity (K_i) of 919 nM while maintaining low nM binding affinities for both the hNK-3R ($K_i = 1.5$ nM) and hNK-2R ($K_i = 4.6$ nM).

This trend in SARs was also verified in another amide series, featuring the (*S*)-1-cyclohexylethylamine. As with **10**, compound **21** (incorporating the piperazinylmethyl group at position 3 of the quinoline ring) showed a high binding affinity for both the hNK-3R ($K_i = 3.4$ nM) and hNK-2R ($K_i = 2.4$ nM) and similar human μ-opioid receptor binding affinity ($K_i = 172$ nM).

Again, when the nitrogen position is shifted as in compounds **23**−**25,** the human μ-opioid binding affinity was significantly reduced or even essentially abolished (it ranged from 1322 to >2500 nM).

In particular, compound **25**, featuring the 4-(morpholin-4-yl)piperidin-1-yl derivative, showed an impressive binding profile and can be considered as a viable pharmacological tool to assess the therapeutic potential of combined NK-3 and NK-2 receptor antagonists. In fact, in addition to the exquisite selectivity over the μ-opioid receptor (human μ-opioid receptor binding affinity, $K_i > 2.5$ μM), **25** diplayed very high hNK-3R ($K_i = 0.8$ nM) and hNK-2R ($K_i = 0.8$ nM) binding affinities. Docking studies (Figure 5) showed that the oxygen of the morpholine ring was able to pick up a hydrogen bond with a conserved serine at the top of TM4 (**S**170 in NK-2R/**S**222 in NK-3R) and a conserved histidine (**H**198 in NK-2R/**H**248 in NK-3R) at the top of TM5. A lack of any significant binding affinity for the κ- and δ-opioid receptors completed the in vitro biological profile.

A further validation of the SAR hypothesis explaining the μ-opioid component on the basis of the nitrogen

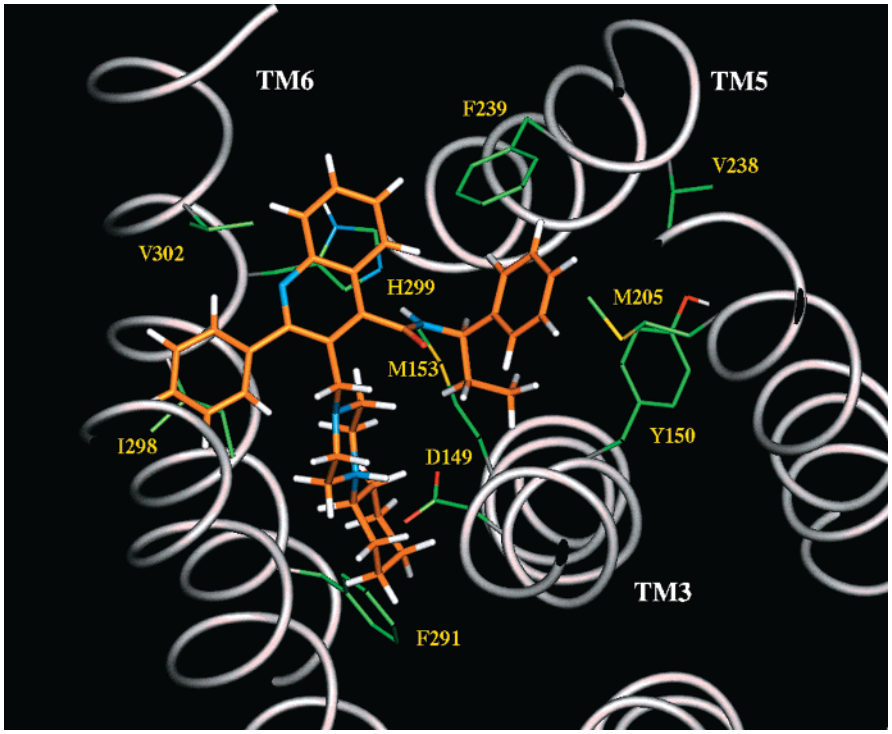

Figure 3. Docking of compound **12** in the human μ-opioid receptor model. The protonated nitrogen is interacting with aspartate (**D**149) in TM helix 3. Note that this orientation is essentially inverted with respect to the neurokinin docking mode.

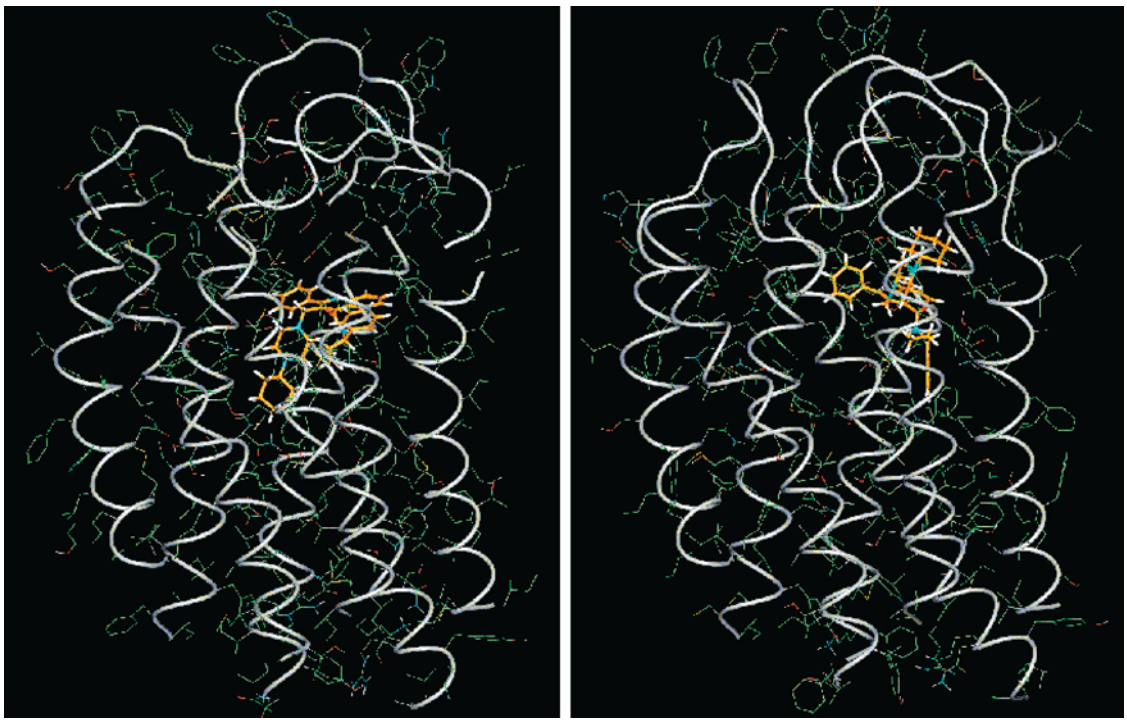

Figure 4. Side view of compound **12** in the NK-2 (right) and human μ-opioid (left) receptor models showing the different binding orientations. The extracellular side is on the top of the picture.

position and its basic nature was given by the inactivity at the human μ-opioid receptor of compounds **26** (lack of the second piperazine basic nitrogen) and **27** (lack of the basic nature of the second piperazine nitrogen). Both **26** and **27** showed binding affinities for the hNK-3 and hNK-2 receptors lower than 6.1 nM.

Finally, to obtain also a selective hNK-2R compound with no opioid receptor binding affinity, we decided to combine the 4-(piperidin-1-yl)piperidin-1-yl basic moiety with a variety of amides possessing those features believed to be crucial in minimizing the hNK-3R component while maintaining a strong hNK-2R binding affinity. Compound **28**, featuring the (*S*)-3,3-dimethylbut-2-yl residue, was found to be the most selective antagonist among all the compounds synthesized, showing a hNK-2R binding affinity of 1.0 nM (K_i), a hNK-2/

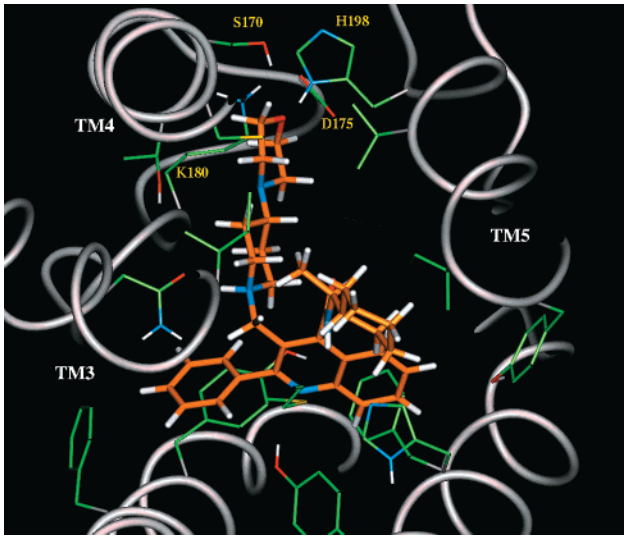

Figure 5. Compound **25** docked in the NK-2 receptor model. Note the additional interactions of the morpholine oxygen with serine (**S**170) and histidine (**H**198).

hNK-3 receptor binding affinity ratio of 0.005, and human μ-opioid receptor binding affinity greater than 2000 nM (K_i).

Conclusions

In this paper, optimization of the combined hNK-3 and hNK-2 receptor profile of compounds **1, 6**−**8, 10**−**19, 21**, and **23**−**28** by means of stepwise chemical modifications was presented. This optimization was carried out in conjunction with docking studies, using novel receptor models that were based on de novo folding of the TM helices around published electron density information. Another key feature of the models was the inclusion of the extracellular loops that were built using a novel combined distance geometry−locally enhanced sampling (LES) simulation method. The optimization process was conducted by starting from compounds **1** and **6**, which displayed a hNK-3R-selective profile. Two portions of the molecule, where modeling has suggested that differences in the receptors could be utilized (namely, the basic group at position 3 and the amide at position 4 of the quinoline ring), were broadly investigated.

The introduction of a basic, sterically hindered and cyclized group at position 3 increased the hNK-2R component. However, incorporation of the piperazine group (compounds **10**−**18** and **21**) resulted in a significant μ-opioid binding interaction that was attributed to the nonbenzylic piperazine nitrogen. As suggested by docking studies, this issue was overcome by a simple shift of the position of this nitrogen (compounds **19**, **23**−**25**, and **28**) or by removal of its basic nature (compound **27**).

Substituents on the amidic portion proved to be crucial with regard to affinity for the hNK-3R, thus allowing the modulation of the neurokinin selectivity profile. In particular, compounds lacking the benzyl or cyclohexylmethyl groups had significantly lower affinity for the hNK-3R. Whereas (*S*)-(+)-*N*-(1-cyclohexylethyl)-3-[(4-morpholin-4-yl)piperidin-1-yl]methyl-2-phenylquinoline-4-carboxamide (compound **25**, SB-400238, hNK-3R binding affinity, K_i = 0.8 nM; hNK-2R binding affinity, K_i = 0.8 nM) emerged as the best example of combined NK-3 and NK-2 receptor antagonist, (*S*)-(+)-*N*-(1,2,2-trimethylpropyl)-3-[(4-piperidin-1-yl)piperidin-1-yl]methyl-2-phenylquinoline-4-carboxamide (compound **28**, SB-414240, hNK-3R binding affinity, K_i = 193 nM; hNK-2R binding affinity, K_i = 1.0 nM) was found to be the most NK-2R-selective. Both these compounds are devoid of any significant affinity for the μ, δ, and κ-opioid receptors.

On the basis of the above considerations we have demonstrated the possibility of utilizing a common chemical template to modulate the NK-2 and NK-3 receptor affinity and selectivity by subtle chemical modifications.

Compounds **25** and **28** join compound **1** as viable pharmacological tools that will be used to better elucidate the pathophysiological role of the NK-3 and NK-2 receptors and to clarify the therapeutic potential of NK-3R-selective, NK-2R-selective, or the combined antagonists at both these receptors.

Footnote

While the design work described above was carried out on theoretical models of the receptors, during the time of writing, the first X-ray crystal structure of a GPCR, viz., bovine rhodopsin, was published.[43] Comparison of our theoretical models with homology models of the receptors showed that they were in fact very close in structure. TM helices 3, 6, and most of 7 aligned almost perfectly with the crystal-based models. Helices 1 and 2 were correctly oriented toward the inner face of the bundle but were approximately displaced by one helical turn in the transmembrane axis. Helices 4 and 5 were correct in their placement in the membrane axis, but the inward faces were out by approximately 60°. The overall result was that the binding pocket described above was largely unchanged. For NK-3R, tyrosine (**Y**315), phenylalanine (**F**319), and histidine (**H**316) still form the main binding pocket for the quinoline ring. The 3-phenyl substituent remains in a pocket bounded by asparagine (**N**162), proline (**P**165), tyrosine (**Y**338), and phenylalanine (**F**342). The asparagine can still form a hydrogen bond with the protonated nitrogen. The only major difference between our theoretical model and the crystal-based homology model is in the binding pocket for the hydrophobic substituent on the 4-amido group. On one side, the TM3 residues isoleucine (**I**166), valine (**V**169), and phenylalanine (**F**170) remain in the same orientation. However, the differing orientation of TM5 means that the role of valine (**V**255) in NK-3R is replaced by tyrosine (**Y**256). However, the differing selectivities in this pocket can still be explained by the valine (**V**169 in NK3) to methionine (NK-2R) change as described earlier. While the TM helices of GPCR models can be placed with much greater confidence as a result of the crystal structure, the extracellular loop regions would be expected to have much greater flexibility. The deeply buried second extracellular loop of rhodopsin is unlikely to be mimicked by other antagonist bound receptors because such ligands would have no access to the binding pocket. Loop modeling, as described earlier, is still therefore necessary in the consideration of GPCR homology structures and their ligand docking.

Experimental Section

1. Radioligand Binding Assay. Neurokinin Receptors. The CHO cells expressing the hNK-1, hNK-2, and hNK-3 receptors were cultured at 37 °C in a humidifier incubator under 5% CO_2/95% air in 1017 SO_3 (in-house formulation) media containing nucleosides plus Geneticin (400 mg/L). The cells were harvested by centrifugation at 600 *g* for 10 min. The cell pellet was resuspended in hypotonic buffer (10 mM Tris, pH 7.4, 1.0 mM EDTA, 10 μg/mL soybean trypsin inhibitor, 100 μg/mL bacitracin, 100 μM benzamidine, and 10 μM phenylmethylsulfonyl fluoride), and the mixture was then rapidly frozen and thawed (3 times) followed by Dounce homogenization for preparation of crude membranes. For NK-3R competition binding studies,[15] membranes (~15 μg protein) were incubated with 0.15 nM [^{125}I]-[MePhe^7]-NKB in a total of 150 μL of 50 mM Tris, pH 7.4, 4 mM $MnCl_2$, 1 μM phosphoramidon, and 0.1% ovalbumin, with or without various concentrations of antagonist, for 90 min at 25 °C. Incubations were stopped by rapid filtration with a Brandell tissue harvestor (Gaithersburg, MD) through Whatman GF/C filters that were presoaked for 60 min in 0.5% bovine serum albumin (BSA). Membranes were washed with 10 mL of ice cold 20 mM Tris, pH 7.4 containing 0.1% BSA, then placed in vials with 10 mL of Beckman "Ready Safe" and counted in a Beckman LS 6000 (Fullerton, CA) liquid scintillation counter. Specific binding was determined by subtracting total binding from nonspecific binding, which was assessed as the binding in the presence of 0.5 μM cold [MePhe^7]-NKB.

For NK-2R competition binding studies,[16] cells were grown and membranes were prepared as described above for the hNK-3R binding assay. The assay buffer was the same as that utilized for the hNK-3R binding assay with a total volume of 150 μL, ~10 μg of membrane protein and 0.15 nM [^{125}I]-NKA, which was incubated for 90 min at 25 °C, with various concentrations of antagonist. Filtration was through Whatman GF/C filters soaked for 30 min in 0.1% polyethylenimine (PEI), and membranes were washed as described above for the hNK-3R binding assay. Nonspecific binding was determined in the presence of 0.5 μM cold NKA. For NK-1R competition binding studies,[17] the assay volume was 300 μL and the assay buffer (25 mM Tris, pH 7.4, 2.0 mM $CaCl_2$, 2.0 mM $MgCl_2$, 1 μM phosphoramidon, and 0.1% ovalbumin) contained various concentrations of antagonist and 1.0 nM [^{3}H]-substance P. Membranes were incubated for 45 min at 25 °C; Whatman filters were presoaked with BSA and membranes washed as described for the hNK-3R binding assay. Nonspecific binding was determined in the presence of 1 μM cold substance P and K_i determined as for the NK-3 and NK-2 receptor binding assays.

2. Opioid Receptors. CHO cells expressing the hDOR and hMOR were grown in suspension culture in serum-free media (1017 SO_3) in the presence of 0.05% pluronic acid (F18) and maintained at 37 °C and gassed with 5% CO_2. Selection for CHO transfectants was performed by growth in the absence of nucleotides. The maximum cell density for these cell lines was 4×10^6 cells/mL. From binding studies it was determined that transfected CHO cell lines express hDOR and hMOR at a density of 11.5 and 6.9 pmol/mg protein, respectively.

HEK-293 cells expressing hKOR were grown attached to T-150 flasks in Earles's minimum essential medium (E-MEM) supplemented with 10% FBS and 2 mM L-glutamine; G418 was included for selection. The stable cell line expresses hKOR at a density of 3.6 pmol/mg protein from binding studies.

Cells were harvested in phosphate-buffered saline (1×10^6 cells/ mL) and collected by centrifugation (800 *g* for 5 min). The pellets were resuspended in the same volume of ice-cold 10 mM potassium phosphate buffer pH 7.2 (buffer A) and centrifuged at 40 000 *g* for 10 min. The cells were hypoosmotically lysed by resuspension in the same volume of buffer A for 20 min in ice and centrifuged at 800 *g* (5 min), saving the supernatant. The resulting pellets were resuspended in buffer A, and the last step was repeated two more times, saving supernatants each time. Supernatants derived from the three low-speed centrifugations were pooled and centrifuged at the high speed. Pellets were resuspended in buffer A containing 0.32 M sucrose and 5 mM EDTA (buffer B) to wash and concentrate the membranes. The final pellets were resuspended in buffer B at a final concentration of 1−2 mg protein/mL (ca. 40×10^6 cells/mL) and stored at −80 °C. Protein was determined with the protein assay kit from Sigma Chemical Co. (Milan, Italy). $MgCl_2$ (3 mM) was added to buffer A in the case of cells expressing hMOR and hKOR.

Binding experiments were performed in triplicate at a final protein concentration of 10 μg/mL in buffer A and a radiolabeled ligand concentration of 0.4−0.5 nM. The nonspecific binding was determined in the presence of naloxone 10 μM and under these assay conditions was less than 1% of the radioligand added. Samples (final volume of 2 mL) were incubated for 60 min at 37, 30, and 25 °C for δ-, μ-, and κ-receptor binding assays, respectively. The reaction was terminated by rapid filtration through Whatman GF/B filters and two washes with cold assay buffer A (4 mL) using a M48 Brandel cell harvester (Biomedical Research and Development Laboratories, Inc., Gaithersburg, MD). Filters used for [^{3}H]-U69593 binding were presoaked in buffer A containing 0.05% polyethylenimine. Radioactivity on the filters was measured by liquid scintillation counting with a Camberra Packard 2500TR β counter (Milan, Italy).

3. Computational Chemistry. 3.1. General. Visualization of the density maps, the various receptor models, and their ligands, as well as the generation of the initial rhodopsin model and the manual docking of the ligands, was carried out with the program Quanta.[37] Molecular mechanics energy refinements, minimizations, and molecular dynamics simulations were performed with the program CHARMm.[38] Ligand molecules were built using the builder option of the program Spartan.[41] They were further optimized at the semiempirical level with the Vamp program,[44] using the AM1 Hamiltonian and suitable symmetry constraints to maintain planar amide bonds. The atom-centered charges for the ligands, used in the docking studies, were natural atomic orbital charges calculated at the Hartree−Fock level within Spartan, using a 3-21G* basis set. The electrostatic potential calculations used in the estimation of relative basicities were also carried out with Spartan at the same level. Following manual docking of the ligands into the receptor models, they were minimized with CHARMm using a distance-dependent dielectric and 1000 steps of steepest descent, followed by 5000 steps of ABNR. Generation of the transmembrane helical bundles of the NK-2, NK-3, and μ-opioid receptor models from the rhodopsin template was done with the GPCR_Builder program.[35]

3.2. Generation of the Extracellular Loops. A semiautomated procedure for the generation of the extracellular loops has been developed. Initial conformational sampling was performed using the distance geometry program DGEOM95.[45] Distance constraints were automatically derived from the N- and C-terminal helical five residues, together with the disulfide bond information in the case of the second extracellular loop and appropriate steric information from previously generated loops. Typically 500 random conformations were generated. A modification to the DGEOM95 program allowed the application of the Karplus rotamer library[36] prior to export of the files. Each loop structure was minimized with CHARMm using 1000 steps of steepest descent and 5000 steps of ABNR. A constant dielectric of 7 was used in this case to decrease the influence of electrostatic terms. The conformations were analyzed by goodness of backbone $\phi-\psi$ angles using the criteria described by Wilmot et al.[46] They were clustered by backbone dihedral "families" and further ranked by energy.The best conformations were chosen for subsequent molecular dynamics analysis using the locally enhanced sampling (LES) method of Elber,[47] as utilized in CHARMm. Following heating and equilibration at 400 K, the loops were run for 250 ps, and the trajectories were again analyzed by backbone $\phi-\psi$ angles. The best resulting conformations were further minimized as described above.

3.3. Derivation of the Three-Dimensional Density Slices. The images from the paper of Unger et al.[24a] were

scanned into the computer and were then converted to pure black and white 24 bit (8 bit each of red, green, and blue) formatted bitmap postscript files. These have the white represented as "ffffff" in hexadecimal notation and the black as "000000". The computer program written to convert these files into three-dimensional information searched each line of the image, noting the coordinates of the midpoint of any transition from white to black to white. These were interpreted as points on the density contour lines. Adjacent points were then connected using a simple distance search algorithm, and the coordinates of the points were converted to angstroms using the scale factor in the original paper. The density information for each slice was then written as a formatted "QM coordinate" file suitable for input into the Quanta program.

4. Synthetic Chemistry. Melting points were determined with a Büchi 530 hot stage apparatus and are uncorrected. Proton NMR spectra were recorded on a Bruker ARX 300 spectrometer at 303 K unless otherwise indicated. Chemical shifts were recorded in parts per million (δ) downfield from tetramethylsilane (TMS); NMR spectral data are reported as a list. IR spectra were recorded in Nujol mull or neat on sodium chloride disks or in KBr with a Perkin-Elmer 1420 spectrophotometer; mass spectra were obtained on a Finnigan MAT TSQ-700 (or TSQ 70) spectrometer. Optical rotations were determined in MeOH solution at the indicated concentration with a Perkin-Elmer 341 polarimeter at the sodium D-line. Silica gel used for flash column chromatography was Kiesegel 60 (230−400 mesh) (E. Merck AG, Darmstadt, Germany). Evaporations were performed at reduced pressure, and all oily products were dried at 0.1 mbar for 16 h. Combustion elemental analyses were performed by Redox s.n.c., Milan, Italy, and values found were within 0.4% of the theoretical values (unless otherwise indicated).

Tetrahydrofuran (THF) was dried by distillation over $LiAlH_4$ and stored over 4 Å molecular sieves under nitrogen atmosphere; DCM was dried over $CaCl_2$; MeCN and DMF were stored over 4 Å molecular sieves. Triethylamine (TEA) was dried by distillation and stored over KOH. Amines RH, where R has the meanings reported in Scheme 1 for compounds **5a**−**g** and **5i**, are commercially available compounds; 4-piperidin-4-ylmorpholine was prepared according to Freifelder et al.,[48] and 2-methyl-1-piperazin-1-ylpropan-1-one was prepared according to Meyer et al.[49] Amines R_1H, where R_1 has the meanings reported in Scheme 1 for compounds **6, 8**−**12**, and **14**−**28**, are commercially available compounds; (*S*)-2-methyl-1-phenylpropylamine was prepared according to Pallavicini et al.[50] Compound **2** is a commercially available compound or can be prepared according to the synthetic procedure reported by Giardina et al.[11]

5. Synthesis of Intermediates. 5.1. Methyl 3-Methyl-2-phenylquinoline-4-carboxylate (3). 3-Methyl-2-phenylquinoline-4-carboxylic acid (**2**, 30 g, 114 mmol, CAS [43071-45-0]) were suspended in dry DCM (250 mL); oxalyl chloride (20 mL, 230 mmol) dissolved in DCM (120 mL) was added dropwise, and the reaction mixture was stirred at room temperature for 30 min. Two drops of DMF were added, and the reaction was stirred for an additional 30 min. The solvent was evaporated to dryness, the residue was taken up with DCM (100 mL), and MeOH (100 mL) dissolved in DCM (400 mL) was added dropwise. After the mixture was stirred for 18 h, the solvent was evaporated to dryness and the residue was taken up with DCM and washed with 1% $NaHCO_3$. The organic layer was dried over anhydrous Na_2SO_4, filtered, and evaporated to dryness to yield **3** (31.4 g, 113 mmol, 99%) as a solid, which was used in the following reaction without further purification; mp 73−75 °C. IR (KBr): 3441, 3051, 2954, 1731, 1582, 1556 cm^{-1}. ^1H NMR ($CDCl_3$): δ 8.15 (d, J = 8.0 Hz, 1H), 7.73 (m, 2H), 7.62−7.40 (m, 7H), 4.10 (s, 3H), 2.40 (s, 3H). EI-MS (source 180 °C, 70 eV, 200 mA): m/z 277 ($M^{+\bullet}$), 276, 262, 246, 217, 166.

5.2. Methyl 3-Bromomethyl-2-phenylquinoline-4-carboxylate (4). Methyl 3-methyl-2-phenyl-quinoline-4-carboxylate (**3**, 10 g, 36 mmol) was dissolved in CH_3CN (500 mL); *N*-bromosuccinimide (13 g, 72 mmol) was added, and the reaction mixture was heated to reflux. After the addition of dibenzoylperoxide (1 g, 4.1 mmol), the reaction was refluxed for 24 h, then additional *N*-bromosuccinimide (4 g, 22.5 mmol) and dibenzoylperoxide (0.5 g, 2.0 mmol) were added, and the reaction was refluxed for 4 h. The solvent was evaporated to dryness, and the residue was taken up with EtOAc and washed with H_2O, 5% $NaHCO_3$, and H_2O. The organic layer was dried over anhydrous Na_2SO_4, filtered, evaporated to dryness, and triturated with Et_2O to yield **4** (9.0 g, 25.3 mmol, 70%) as a white solid; mp 118−120 °C. IR (KBr): 3453, 3062, 3037, 2952, 1735, 1575, 1556 cm^{-1}. ^1H NMR (DMSO): δ 8.09 (d, J = 8.0 Hz, 1H), 7.89 (d, J = 8.0 Hz, 2H), 7.88 (dd, J = 8.0, 8.0 Hz, 1H), 7.73 (dd, J = 8.0, 8.0 Hz, 1H), 7.67 (m, 2H), 7.55 (m, 3H), 4.69 (s, 2H), 4.11 (s, 3H). EI-MS (source 180 °C, 70 eV, 200 mA): m/z 355 ($M^{+\bullet}$), 276, 232, 216.

5.3. General Procedure for the Synthesis of Compounds 5a−j in Scheme 1. Methyl 3-bromomethyl-2-phenylquinoline-4-carboxylate (**4**, 5 g, 14 mmol), amine RH (where R has the meanings reported in Scheme 1 for compounds **5a**−**j**) (15.4 mmol), and ethyldiisopropylamine (2.7 mL, 15.4 mmol) were dissolved in dry THF (100 mL), and the mixture was stirred for 1 night at 50 °C. The solvent was concentrated, the residue was dissolved in CH_2Cl_2 and washed with water, and the organic phase was dried over $MgSO_4$. After concentration of the solvent, the residue was purified by flash column chromatography over silica gel, affording compounds **5a**−**j** in 50−80% yield.

As an example, spectroscopic data of compound **5f** are reported. Mp 118−120 °C. IR (KBr): 3572, 3054, 2968, 2935, 2784, 1715, 1573, 1556 cm^{-1}. ^1H NMR (DMSO): δ 8.06 (d, J = 8.8 Hz, 1H), 7.86 (d, J = 8.8 Hz; 1H), 7.81 (dd, J = 8.8, 8.8 Hz, 1H), 7.68 (dd, J = 8.8, 8.8 Hz, 1H), 7.51 (m, 5H), 3.98 (s, 3H), 3.61 (s, 2H), 2.67−2.58 (m, 2H), 2.60−2.35 (m, 4H), 2.11 (m, 1H), 1.78 (m, 2H), 1.62−1.28 (m, 10H). ESI-MS (positive, solvent methanol, spray 4.5 keV, skimmer 60 eV, capillary 220 °C): m/z 444 (MH^+).

6.0. Synthesis of Final Compounds. 6.1. General Procedure for the Synthesis of Compounds 6−9, 11−20, 22, and 24−28. Compounds **5a**−**j** (7.9 mmol) and 6 N HCl (50 mL) were refluxed for 4 h and then concentrated to dryness. The residue was triturated with diethyl ether to obtain the corresponding carboxylic acids, which were used without further purification in the coupling step. These carboxylic acids (7.9 mmol), amines R_1H (where R_1 has the meanings reported in Scheme 1 for compounds **6**−**28**) (12.6 mmol), HBTU (4.8 g, 12.6 mmol), and TEA (5.1 mL, 37 mmol) were dissolved in THF (100 mL) and DCM (25 mL), and the mixture was refluxed for 18 h. The solvent was evaporated, and the residue was dissolved in DCM and washed with H_2O, 0.5 N NaOH, and H_2O. The organic phase was dried over $MgSO_4$, filtered, and evaporated to dryness. The residue was purified by flash column chromatography, affording compounds **6**−**9, 11**−**20, 22**, and **24**−**28** in 60−85% yield. In some cases the free base was dissolved in acetone and acidified with Et_2O saturated with HCl to obtain the corresponding dihydrochloride or trihydrochloride.

As an example, spectroscopic data of compound **24** are reported. Mp 180-184 °C. $[\alpha]_D^{20}$ +6.9° (*c* 0.5, MeOH). IR (KBr): 3422, 2928, 2852, 2659, 1647, 1546 cm^{-1}. ^1H NMR (DMSO; free base): δ 8.27 (d br, J = 8.5 Hz; 1H), 8.01 (d, J = 8.2 Hz, 1H), 7.86 (d, J = 8.2 Hz, 1H), 7.75 (dd, J = 8.2, 8.2 Hz, 1H), 7.62 (dd, J = 8.2, 8.2 Hz, 1H), 7.55 (m, 2H), 7.50−7.42 (m, 3H), 4.09−3.98 (m, 1H), 3.56 (s, 2H), 2.52 (m, 2H), 2.34 (m, 4H), 2.03−1.93 (m, 1H), 1.88−1.60 (m, 6H), 1.56−1.05 (m, 17H), 1.20 (d, J = 6.9 Hz, 3H). EI-MS (source 180 °C, 70 eV, 200 mA): m/z 538 ($M^{+\bullet}$), 372, 261, 167. Anal. ($C_{35}H_{46}N_4O\cdot 3HCl$) C, H, N, Cl.

6.2. General Procedure for the Synthesis of Compounds 10, 21, and 23. Fmoc deprotection of compounds **9**, **20**, and **22** was obtained by dissolving these compounds in CH_3CN, adding piperidine (1.5 equiv), and stirring them at room temperature overnight. Evaporation to dryness and purification by flash column chromatography afforded the

corresponding deprotected compounds **10**, **21**, and **23** in nearly quantitative yields.

As an example, spectroscopic data of compound **21** are reported. Mp 112−114 °C. $[\alpha]_D^{20}$ +20.5 (*c* 1, MeOH). IR (Nujol): 3250, 3100, 1650, 1550, 1470. ^{1}H NMR (DMSO): δ 8.51 (d br, J = 8.5 Hz, 1H), 8.01 (d, J = 8.2 Hz, 1H), 7.84 (d, J = 8.2 Hz, 1H), 7.77 (dd, J = 8.2, 8.2 Hz, 1H), 7.64 (dd, J = 8.2, 8.2 Hz, 1H), 7.57 (m, 2H), 7.50−7.42 (m, 3H), 4.07−3.95 (m, 1H), 3.51 (s, 2H), 2.41 (m, 4H), 2.02 (m, 4H), 1.86−1.60 (m, 5H), 1.54−1.42 (m, 1H), 1.32−0.99 (m, 6H), 1.17 (d, J = 6.9 Hz, 3H). EI-MS (source 180 °C, 70 eV, 200 mA): *m*/*z* 456 ($M^{+\bullet}$), 372, 302, 261, 218, 217. Anal. ($C_{29}H_{36}N_4O$) C, H, N.

Acknowledgment. We are grateful to Roberto Rigolio, Davide Graziani, Lorenzo Perugini, Alberto Cerri, and Renzo Mena (SmithKline Beecham SpA, Italy) for synthetic assistance and mass and NMR spectroscopic determinations. We also thank Isabelle Leger, Isabelle Delimoge, and Marcel Morvan (SmithKline Beecham Laboratoires Pharmaceutiques, France) for NMR and synthetic assistance.

Supporting Information Available: Detailed spectroscopic data (IR, MS, and ^{1}H NMR) for compounds **6**−**8**, **10**−**19**, **21**, and **23**−**28**. This material is available free of charge via the Internet at http://pubs.acs.org.

References

(1) Regoli, D.; Boudon, A.; Fauchere, J.-L. Receptors and antagonists for substance P and related peptides. *Pharmacol. Rev.* **1994**, *46*, 551−599.

(2) Giardina, G. A. M.; Raveglia, L. F.; Grugni, M. Lead generation and lead optimization processes in the discovery of selective nonpeptide neurokinin receptor antagonists. *Drugs Future* **1997**, *22*, 1235−1257.

(3) Gao, Z.; Peet, N. P. Recent advances in neurokinin receptor antagonists. *Curr. Med. Chem.* **1999**, *6*, 375−388.

(4) Von Sprecher, A.; Gerspacher, M.; Anderson, G. P. Neurokinin antagonists as potential therapies for inflammation and rheumatoid arthritis. *IDrugs* **1998**, *1*, 73−91.

(5) Swain, C. J. Neurokinin receptor antagonists. In *Progress in Medicinal Chemistry*; Ellis, G. P., Luscombe, D. K., Oxford, A. W., Eds.; Elsevier Science B.V.: Amsterdam, 1998; Vol. 35, pp 57−81.

(6) Seward, E. M.; Swain, C. J.; Neurokinin receptor antagonists. *Expert Opin. Ther. Pat.* **1999**, *9*, 571−582.

(7) Giardina, G. A. M.; Grugni, M.; Raveglia, L. F. Recent advances in neurokinin-3 receptor antagonists. *Expert Opin. Ther. Pat.* **2000**, *10*, 939−960.

(8) (a) Burkholder, T. P.; Maynard, G. D.; Kudlacz, E. M. (Assignor to Hoechst Marion Roussel, Inc.). Novel carboxy substituted cyclic carboxamide derivatives. International Patent WO/9827085, 1998; *Chem. Abstr.* **1998**, *129*, 95498. (b) Reichard, G. A.; Alaimo, C. A.; Shih, N.-Y.; Ting, P. C.; Carruthers, N. I.; Lavey, B. J. (Assignor to Schering Corp.). Substituted oximes as neurokinin antagonists. U.S. Patent 6,063,926, 2000; *Chem. Abstr.* **2000**, *132*, 334363. (c) Esser, F.; Schnorrenberg, G.; Dollinger, H.; Lüttke, S.; Jung, B.; Speck, G. (Assignor to Boehringer Ingelheim Pharma KG). Novel neurokinin antagonists, method for the production thereof, and pharmaceutical composition containing said compounds. International Patent DE/19824470, 1999; *Chem. Abstr.* **1999**, *132*, 12330. (d) Nishi, T.; Yamaguchi, T.; Iio, Y.; Takemoto, T.; Nakajima, K. (Assignor to Sankyo Co. Ltd.). Spiropiperidine derivatives. International Patent WO/9937642, 1999; *Chem. Abstr.* **1999**, *131*, 116241.

(9) Myers, A. C.; Undem, B. J. Electrophysiological effects of tachykinins and capsaicin on guinea-pig bronchial parasympathetic neurones. *J. Physiol.* **1993**, *470*, 665−679.

(10) Maggi, C. A. Tachykinins in the autonomic nervous system. *Pharmacol. Res.* **1996**, *33*, 161−170.

(11) Giardina, G. A. M.; Raveglia, L. F.; Grugni, M.; Sarau, H. M.; Farina, C.; Medhurts, A. D.; Graziani, D.; Schmidt, D. B.; Rigolio, R.; Luttmann, M.; Cavagnera, S.; Foley, J. J.; Vecchietti, V.; Hay, D. W. P. Discovery of a novel class of selective non-peptide antagonists for the human neurokinin-3 receptor. 2. Identification of (S)-N-(1-phenylpropyl)-3-hydroxy-2-phenylquinoline-4-carboxamide (SB 223412). *J. Med. Chem.* **1999**, *42*, 1053−1065.

(12) Sarau, H. M.; Griswold, D. E.; Potts, W.; Foley, J. J.; Schmidt, D. B.; Webb, E. F.; Martin, L. D.; Brawner, M. E.; Elshourbagy, N. A.; Medhurst, A. D.; Giardina, G. A. M.; Hay, D. W. P. Nonpeptide tachykinin receptor antagonists. I. Pharmacological and pharmacokinetic characterization of SB 223412, a novel, potent and selective NK-3 receptor antagonist. *J. Pharmacol. Exp. Ther.* **1997**, *281*, 1303−1311.

(13) Giardina, G. A. M.; Sarau, H. M.; Farina, C.; Medhurst, A. D.; Grugni, M.; Foley, J. J.; Raveglia, L. F.; Schmidt, D. B.; Rigolio, R.; Vassallo, M.; Vecchietti, V.; Hay, D. W. P. 2-Phenyl-4-quinolinecarboxamides: A Novel Class of Potent and Selective Non-Peptide Competitive Antagonists for the Human Neurokinin-3 Receptor. *J. Med. Chem.* **1996**, *39*, 2281−2284.

(14) Giardina, G. A. M.; Sarau, H. M.; Farina, C.; Medhurst, A. D.; Grugni, M.; Raveglia, L. F.; Schmidt, D. B.; Rigolio, R.; Luttmann, M.; Vecchietti, V.; Hay, D. W. P. Discovery of a novel class of selective non-peptide antagonists for the human neurokinin-3 receptor. 1. Identification of the 4-quinolinecarboxamide framework. *J. Med. Chem.* **1997**, *40*, 1794−1807.

(15) Sadowski, S.; Huang, R.-R. C.; Fong, T. M.; Marko, O.; Cascieri, M. A. Characterization of the Binding of [^{125}I-Iodo-histidyl, methyl-Phe^7] Neurokinin B to the Neurokinin-3 Receptor. *Neuropeptides* **1993**, *24*, 317−319.

(16) Aharony, D.; Conner, G. E.; Woodhouse, D. P. Pharmacologic Characterization of the Novel Ligand [4,5-^{3}H-Leu^9]-Neurokinin-A Binding to NK-2 Receptors on Hamster Urinary Bladder Membranes. *Neuropeptides* **1992**, *23*, 121−130.

(17) Payan, D. G.; McGillis, J. P.; Organist, M. L. Binding Characteristics and Affinity Labeling of Protein Constituents of the Human IM-9 Lymphoblast Receptor for Substance P. *J. Biol. Chem.* **1986**, *261*, 14321−14329.

(18) Kotzer, C. J.; Hay, D. W. P.; Dondio, M.; Giardina, G. A. M.; Petrillo, P.; Underwood, D. The antitussive activity of *delta* opioid receptor stimulation in guinea pigs. *J. Pharmacol. Exp. Ther.* **2000**, *292*, 803−809.

(19) Scheideler, M. A.; Zukin, R. S. Reconstitution of solubilized delta-opiate receptor binding sites in lipidic vesicles. *J. Biol. Chem.* **1990**, *265*, 15176−15182.

(20) Cheng, Y.-C.; Prusoff, W. H. Relationship Between the Inhibition Constant (K_i) and the Concentration of Inhibitor Which Cause 50 Percent Inhibition (IC_{50}) of an Enzymatic Reaction. *Biochem. Pharmacol.* **1973**, *22*, 3099−3108.

(21) (a) Bromidge, S. M.; Dabbs, S.; Davies, D. T.; Davies, S.; Duckworth, D. M.; Forbes, I. T.; Gaster, L. M.; Ham, P.; Jones, G. E.; King, F. D.; Mulholland, K. R.; Saunders, D. V.; Wyman, P. A.; Blaney, F. E.; Clarke, S. E.; Blackburn, T. P.; Holland, V.; Kennett, G. A.; Lightowler, S.; Middlemiss, D. N.; Trail, B.; Riley, G. J.; Wood, M. D. Biarylcarbamoylindolines Are Novel and Selective 5-HT2C Receptor Inverse Agonists: Identification of 5-Methyl-1-[[2-[(2-methyl-3-pyridyl)oxy]- 5-pyridyl]carbamoyl]-6-trifluoromethylindoline (SB-243213) as a Potential Antidepressant/Anxiolytic Agent. *J. Med. Chem.* **2000**, *43*, 1123−1134. (b) Gaster, L. M.; Blaney, F. E.; Duckworth, D. M.; Ham, P.; Jenkins, S.; Jennings, A. J.; Joiner, G. F.; King, F. D.; Mulholland, K. R.; Starr, S.; Wyman, P. A.; Hagan, J. J.; Hatcher, J.; Jones, B. J.; Middlemiss, D. N.; Price, G. W.; Riley, G.; Roberts, C.; Routledge, C.; Selkirk, J.; Slade, P. D. The Selective 5-HT1B Receptor Inverse Agonist 1′-Methyl-5-[[2′-methyl-4′- (5-methyl-1,2,4-oxadiazol-3-yl)biphenyl-4-yl]carbonyl]-2,3,6,7-te trahydrospiro[furo[2,3-f]indole-3,4′-piperidine] (SB-224289) Potently Blocks Terminal 5-HT Autoreceptor Function Both in Vitro and in Vivo. *J. Med. Chem.* **1998**, *41*, 1218−1235.

(22) Bikker, J. A.; Trumpp-Kallmeyer, S.; Humblet, C. G-Protein Coupled Receptors: Models, Mutagenesis, and Drug Design. *J. Med. Chem.* **1998**, *41*, 2911−2927.

(23) Schertler, G. F. X.; Villa, C.; Henderson, R. Projection structure of rhodopsin. *Nature (London)* **1993**, *362*, 770−772.

(24) (a) Unger, V. M.; Hargrave, P. A.; Baldwin, J. M.; Schertler, G. F. X. Arrangement of rhodopsin transmembrane α-helixes. *Nature (London)* **1997**, *389*, 203−206. (b) Baldwin, J. M.; Schertler, G. F. X.; Unger, V. M. An alpha-carbon template for the transmembrane helixes in the rhodopsin family of G-protein-coupled receptors. *J. Mol. Biol.* **1997**, *272*, 144−164.

(25) Kyte, J.; Dolittle, R. F. A simple method for displaying the hydropathic character of a protein. *J. Mol. Biol.* **1982**, *157*, 105−132.

(26) Blundell, T.; Barlow, D.; Borkakoti, N.; Thornton, J. Solvent induced distortions and the curvature of α-helices. *Nature (London)* **1983**, *306*, 281−283.

(27) Blaney, F. E.; Tennant, M. Helanal−A Novel Algorithm for the Construction of Transmembrane Helical Bundles. Poster presented at the International Conference on Protein Folding and Design, Bethesda, MD, 1996. See also ref 35.

(28) Donnelly, D.; Overington, J. P.; Blundell, T. L. The prediction and orientation of α-helixes from sequence alignments: the combined use of environment-dependent substitution tables. Fourier transform methods and helix capping rules. *Protein Eng.* **1994**, *7*, 645−653.

(29) Choudhary, M. S.; Craigo, S.; Roth, B. L. A single point mutation (Phe340→Leu340) of a conserved phenylalanine abolishes 4-[125I]-iodo-(2,5-dimethoxy)phenylisopropylamine and [3H]mesulergine but not [3H]ketanserin binding to 5-hydroxytryptamine2 receptors. *Mol. Pharmacol.* **1993**, *43*, 755−761.
(30) (a) Strader, C. D.; Sigal, I. S.; Register, R. B.; Candelore, M. R.; Rands, E.; Dixon, R. A. F. Identification of residues required for ligand binding to the β-adrenergic receptor. *Proc. Natl. Acad. Sci. U.S.A.* **1987**, *84*, 4384−4388. (b) Mansour, A.; Meng, F.; Meador-Woodruff, J. H.; Taylor, L. P.; Civelli, O.; Akil, H. Site-directed mutagenesis of the human dopamine D2 receptor. *Eur. J. Pharmacol., Mol. Pharmacol. Sect.* **1992**, *227*, 205−214.
(31) Strader, C. D.; Candelore, M. R.; Hill, W. S.; Sigal, I. S.; Dixon, R. A. F. Identification of two serine residues involved in agonist activation of the β-adrenergic receptor. *J. Biol. Chem.* **1989**, *264*, 13572−13578.
(32) Wess, J.; Nanavati, S.; Vogel, Z.; Maggio, R. Functional role of proline and tryptophan residues highly conserved among G protein-coupled receptors studied by mutational analysis of the m3 muscarinic receptor. *EMBO J.* **1993**, *12*, 331−338.
(33) (a) Javitch, J. A.; Li, X.; Kaback, J.; Karlin, A. A cysteine residue in the third membrane-spanning segment of the human D2 dopamine receptor is exposed in the binding-site crevice. *Proc. Natl. Acad. Sci. U.S.A.* **1994**, *91*, 10355−10359. (b) Javitch, J. A.; Fu, D.; Chen, J. Residues in the Fifth Membrane-Spanning Segment of the Dopamine D2 Receptor Exposed in the Binding-Site Crevice. *Biochemistry* **1995**, *34*, 16433−16439. (c) Fu, D.; Ballesteros, J. A.; Weinstein, H.; Chen, J.; Javitch, J. A. Residues in the Seventh Membrane-Spanning Segment of the Dopamine D2 Receptor Accessible in the Binding-Site Crevice. *Biochemistry* **1996**, *35*, 11278−11285. (d) Javitch, J. A.; Ballesteros, J. A.; Weinstein, H.; Chen, J. A Cluster of Aromatic Residues in the Sixth Membrane-Spanning Segment of the Dopamine D2 Receptor Is Accessible in the Binding-Site Crevice. *Biochemistry* **1998**, *37*, 998−1006. (e) Javitch, J. A.; Ballesteros, J. A.; Chen, J.; Chiappa, V.; Simpson, M. M. Electrostatic and Aromatic Microdomains within the Binding-Site Crevice of the D2 Receptor: Contributions of the Second Membrane-Spanning Segment. *Biochemistry* **1999**, *38*, 7961−7968.
(34) (a) Oliveira, L.; Paiva, A. C. M.; Sander, C.; Vriend, G. A common step for signal transduction in G protein-coupled receptors. *Trends Pharmacol. Sci.* **1994**, *15*, 170−172. (b) Sealfon, S. C.; Chi, L.; Ebersole, B. J.; Rodic, V.; Zhang, D.; Ballesteros, J. A.; Weinstein, H. Related contribution of specific helix 2 and 7 residues to conformational activation of the serotonin 5-HT2A receptor. *J. Biol. Chem.* **1995**, *270*, 16683−16688. (c) Perlman, J. H.; Colson, A.-O.; Wang, W.; Bence, K.; Osman, R.; Gershengorn, M. C. Interactions between conserved residues in transmembrane helixes 1, 2, and 7 of the thyrotropin-releasing hormone receptor. *J. Biol. Chem.* **1997**, *272*, 11937−11942.
(35) Blaney, F. E.; Tennant, M. Computational tools and results in the construction of G protein-coupled receptor models. In *Membrane Protein Models*; Findlay, J. B. C., Ed.; Bios Scientific Publishers, Ltd.: Oxford, 1996; pp 161−176.
(36) Dunbrack, R. L., Jr.; Karplus, M. Backbone-dependent rotamer library for proteins. Application to side-chain prediction. *J. Mol. Biol.* **1993**, *230*, 543−574.
(37) *Quanta98*, version 98.1111; Molecular Simulations, Inc.: San Diego, 1999.
(38) Brooks, B. R.; Bruccoleri, R. E.; Olafson, B. D.; States, D. J.; Swaminathan, S.; Karplus, M. CHARMM: a program for macromolecular energy, minimization, and dynamics calculations. *J. Comput. Chem.* **1983**, *4*, 187−217. *CHARMm*, version 25.2, revision 98.0731; Molecular Simulations, Inc.: San Diego, 1999.
(39) Kao, H. T.; Adham, N.; Olsen, M. A.; Weinshank, R. L.; Branchek, T. A.; Hartig, P. R. Site-directed mutagenesis of a single residue changes the binding properties of the serotonin 5-HT2 receptor from a human to a rat pharmacology. *FEBS Lett.* **1992**, *307*, 324−328.
(40) Elling, C. E.; Moeller, N.; Nielsen, S. M.; Schwartz, T. W. Conversion of antagonist-binding site to metal-ion site in the tachykinin NK-1 receptor. *Nature (London)* **1995**, *374*, 74−77.
(41) *SPARTAN SGI*, version 5.1.3; Wavefunction, Inc.: Irvine, CA, 1999.
(42) Edmonds-Alt, X.; Bichon, D.; Ducoux, J. P.; Heaulme, M.; Miloux, B.; Poncelet, M.; Proietto, V.; Van Broeck, D.; Vilain, P.; Neliat, G.; Soubrié, P.; Le Fur, G.; Breliere, J. C. SR 142801, the First Potent Non-Peptide Antagonist of the Tachykinin NK-3 Receptor. *Life Sci.* **1995**, *56*, PL27−PL32.
(43) Polczewski, K.; Kumasaka, T.; Hori, T.; Behnke, C. A.; Motoshima, H.; Fox, B. A.; Le Trong, I.; Teller, D. C.; Okada, T.; Stenkamp, R. E.; Yamamoto, M.; Miyano, M. Crystal structure of rhodopsin: A G protein-coupled receptor. *Science (Washington, D.C.)* **2000**, *289*, 739−745.
(44) Clark, T.; Alex, A.; Beck, B.; Chandrasekhar, J.; Gedeck, P.; Horn, A.; Hutter, M.; Rauhut, G.; Sauer, W.; Steinke, T. *Vamp*, version 7.0; Oxford Molecular, Ltd.: Oxford, 1998.
(45) Blaney, J. M.; Crippen, G. M.; Dearing, A.; Dixon, J. S.; Spellmeyer, D. C. DGEOM95 is available from the Quantum Chemistry Program Exchange, Bloomington, Indiana, 1995.
(46) Wilmot, C. M.; Thornton, J. M. β-Turns and their distortions: a proposed new nomenclature. *Protein Eng.* **1990**, *3*, 479−493.
(47) (a) Elber, R.; Karplus, M. Enhanced sampling in molecular dynamics: use of the time-dependent Hartree approximation for a simulation of carbon monoxide diffusion through myoglobin. *J. Am. Chem. Soc.* **1990**, *112*, 9161−9175. (b) Roitberg, A.; Elber, R. Modeling side chains in peptides and proteins: application of the locally enhanced sampling and the simulated annealing methods to find minimum energy conformations. *J. Chem. Phys.* **1991**, *95*, 9277−9287.
(48) Freifelder, M.; Stone, G. R. Reductions with ruthenium. II. Its use in the hydrogenation of pyridines. *J. Org. Chem.* **1961**, *26*, 3805−3808.
(49) Meyer, W. E.; Tomcufcik, A. S.; Chan, P. S.; Haug, M. 5-(1-Piperazinyl)-1H-1,2,3,4-triazol-3-amines as antihypertensive agents. *J. Med. Chem.* **1989**, *32*, 593−597.
(50) Pallavicini, M.; Valoti, E.; Villa, L.; Piccolo, O. Resolution of amines with isopropylidene glycerol hydrogen phthlate. *Tetrahedron: Asymmetry* **1997**, *8*, 1069−1073.

JM000501V